

Electron trapping and acceleration across a parabolic plasma density profile

J. U. Kim,* N. Hafz, and H. Suk

Korea Electrotechnology Research Institute, Center for Advanced Accelerators, 28-1, Seongju-dong, Changwon 641-120, Korea

(Received 21 July 2003; published 26 February 2004)

It is known that as a laser wakefield passes through a downward density transition in a plasma some portion of the background electrons are trapped in the laser wakefield and the trapped electrons are accelerated to relativistic high energies over a very short distance. In this study, by using a two-dimensional (2D) particle-in-cell (PIC) simulation, we suggest an experimental scheme that can manipulate electron trapping and acceleration across a parabolic plasma density channel, which is easier to produce and more feasible to apply to the laser wakefield acceleration experiments. In this study, 2D PIC simulation results for the physical characteristics of the electron bunches that are emitted from the parabolic density plasma channel are reported in great detail.

DOI: 10.1103/PhysRevE.69.026409

PACS number(s): 52.38.Mf

I. INTRODUCTION

Ever since Tajima and Dawson [1] proposed the possibility of electron acceleration in a plasma, much attention has been paid to plasma-based accelerators such as laser wakefield accelerators (LWFAs) from both theoretical [2,3] and experimental points of view [4,5]. In the conventional LWFA scheme, for electrons to accelerate they should be injected externally by using an external injection accelerator or high-power lasers for optical injection [6,7]. However, in the self-injection cases [8–10], some background electrons in a plasma can be self-injected and the electrons can be accelerated by the laser wakefield to relativistic high energies over a very short distance. Therefore, the major merit of the self-injected LWFA is that it may be built with very compact tabletop size because it does not require auxiliary heavy facilities that most conventional accelerators do. That is why the advanced accelerator community has shown much interest in the self-injection LWFA method in recent years. In the self-modulated (SM) laser wakefield accelerator [9] the laser pulse length L (i.e., $L = c\tau$, where c is the speed of light in free space and τ is the laser pulse duration, respectively) is longer than the plasma wavelength λ_p and for the relativistic self-guiding the laser power P_L should be somewhat larger than the critical power P_c [11]. In a high-plasma density regime, the laser pulse will be axially modulated at the plasma wavelength λ_p because of a self-modulation instability [11]. Another self-injection method was proposed by Bulanov *et al.* [10] based on “wave breaking phenomena,” which occurs as an intense laser pulse undergoes a slowly varying downward density transition with the scale length $L_s \gg \lambda_p$. Recently, Suk *et al.* [8] proposed a self-injection method by using a very sharp downward density transition in a plasma $L_s < \lambda_p$. In this method, the background plasma electrons are trapped and accelerated when a short (less than λ_p), high-energy electron beam passes through the sharp downward density transition. Similar phenomena were observed in simulations when a short, high intensity laser pulse was used instead [12]. From an experimental point of view,

however, it does not seem to be easy to produce either a sharp downward density transition with scale length of $L_s < \lambda_p$ or a slowly varying downward density transition with scale length of $L_s \gg \lambda_p$ in a plasma.

In this paper, we propose an experimental scheme for electron self-injection and acceleration method by using a parabolic plasma density channel, which is easily produced experimentally by intense laser and gas jet interactions. The potential benefit of the proposed work is that it may be readily applicable to LWFA experiments. Although there were some previous LWFA studies performed in a preformed parabolic density channel [13,14], most of the work was conducted along the axis of the channel in which the electron density is minimum to provide optical guiding of an intense laser pulse. In this paper, we report on a simulation of electron trapping and acceleration in a plasma when a short and intense laser pulse passes across a parabolic plasma channel transversely as shown in Fig. 1. As far as we know, this is the first attempt to investigate electron trapping and acceleration across the parabolic plasma density channel. For this purpose, a two-dimensional (2D) particle-in-cell (PIC) simulation was performed by using the fully relativistic and electromagnetic OSIRIS code [14]. The simulation box (i.e., moving window) was assumed to move with the speed of light in free space.

II. SIMULATION PARAMETERS

Figure 1 shows one example of a Mach-Zehnder interferogram of a plasma channel obtained [15] 5 ns after an intense laser pulse and a gas jet interaction [Fig. 1(a)] and its density profile [Fig. 1(b)] across the channel. As shown in Fig. 1(b) the plasma density profile shows a clear density minimum on axis (i.e., $r=0$) and it increases with r and reaches the highest value at the edge where it suddenly decreases to zero with relatively short scale length of $L_s \approx 40 \mu\text{m}$. Assuming the cylindrical symmetry of the plasma channel the density profile shows a typical parabolic shape of $n(r) \approx n_0 + \Delta n r^2 / r_{\text{ch}}^2$. Here, n_0 and Δn are the minimum density on axis and density change, respectively, and r_{ch} is the channel radius. 2D PIC simulations were performed by using this kind of parabolic density channel and the detailed scale length, channel width, and proposed laser propagation direction are illustrated in Fig. 1(a). The full width of the

*Email address: jukim@keri.re.kr

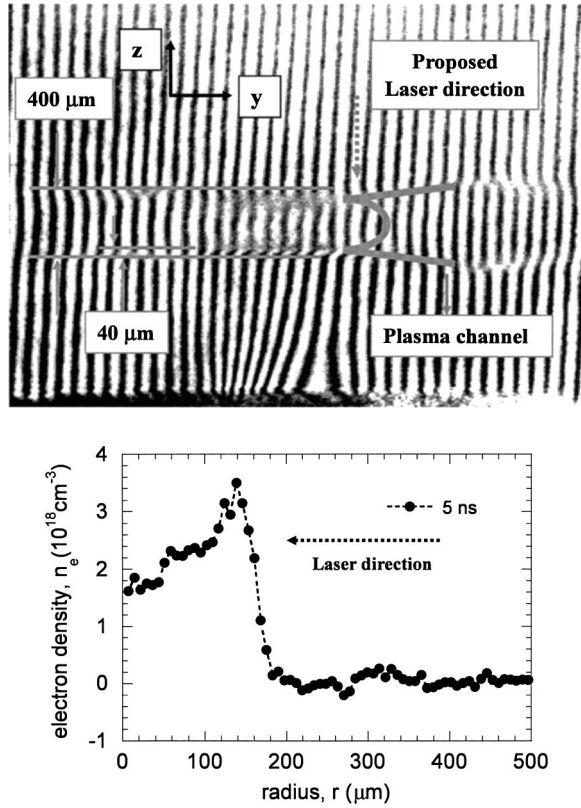


FIG. 1. (a) One example of the Mach-Zehnder interferogram of a plasma channel obtained 5 ns after a laser pulse and gas jet interaction. (b) Electron density profiles of (a). The electron density was measured across the channel shown in (a).

plasma channel and the width of the parabolic density region were fixed to a value of $3140k_0^{-1}$ ($\approx 400 \mu\text{m}$) and $2512k_0^{-1}$ ($\approx 320 \mu\text{m}$), respectively. The edges of the plasma channel were fixed to a value of $314k_0^{-1}$ ($\approx 40 \mu\text{m}$) for both the upward and downward density transitions. Here, k_0 is the wave number of the laser in free space. In order to see the plasma density dependent characteristics, the maximum plasma density used in this simulation was varied from $n_e = 4 \times 10^{18} \text{ cm}^{-3}$ to $n_e = 1 \times 10^{20} \text{ cm}^{-3}$ (i.e., 4×10^{18} , 7×10^{18} , 1×10^{19} , 3×10^{19} , and $1 \times 10^{20} \text{ cm}^{-3}$, respectively) and a fully ionized plasma channel was assumed. The corresponding minimum plasma density used was approximately 43% of its maximum density. Also, a short ($=50 \text{ fs}$, i.e., laser pulse length $L = c\tau \approx 15 \mu\text{m}$) and intense laser pulse (e.g., peak power of the laser $P_L = 10, 20,$ and 30 TW with wavelength of $\lambda_0 = 1.064 \mu\text{m}$) was assumed to pass across the plasma channel as shown in Fig. 1. The normalized vector potential a_0 , which is dependent on the laser power, was set to 2.27, 3.21, and 3.94 and the laser beam was focused at the center of the channel to a spot size of $10 \mu\text{m}$. In this simulation, the laser propagation direction is perpendicular to the axis of the plasma channel as shown in Figs. 1(a) and 1(b).

III. SIMULATION RESULTS AND DISCUSSIONS

Figure 2(a) shows the driving laser pulse and a typical plasma wakefield produced as an intense laser pulse of 20

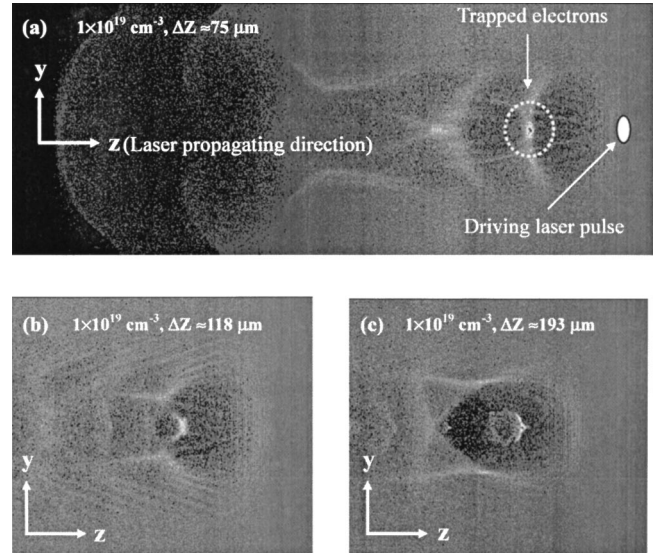


FIG. 2. (a) Electron trapping in the first node of the wakefield at $\Delta Z \approx 588k_0^{-1}$ (i.e., $75 \mu\text{m}$ in the plasma). (b) Injection of the trapped electrons into the acceleration phase of the wakefield at $\Delta Z \approx 924k_0^{-1}$ (i.e., $118 \mu\text{m}$ in the plasma). (c) Further acceleration of the trapped electrons at the downward density transition of the parabolic density profile [i.e., $n(r) \approx n_0 + \Delta n r^2 / r_{\text{ch}}^2$] at $\Delta Z \approx 1512k_0^{-1}$ (i.e., $193 \mu\text{m}$ in the plasma).

TW (i.e., $a_0 \sim 3.21$) passes through the plasma of $1 \times 10^{19} \text{ cm}^{-3}$ at $\Delta Z \approx 588k_0^{-1}$ (i.e., $75 \mu\text{m}$ in the plasma). It is clearly seen that some background electrons are trapped in the first node of the wakefield (i.e., a bright point marked with a dotted circle) as the plasma wakefield passes just down the rim ($\approx 62 \mu\text{m}$) of the parabolic density channel. At further elapsed time, the trapped electrons were injected into the acceleration phase of the wakefield [Fig. 2(b)] and accelerated further [Fig. 2(c)] until they reach almost the minimum density position of $\Delta Z = 1512k_0^{-1}$ (i.e., $\approx 193 \mu\text{m}$) of the parabolic density channel. In general, accelerated electrons are highly relativistic so its velocity is faster than the phase velocity (v_{ph}) of the wakefield, which is nearly equal to the group velocity (v_g) of the driving laser [11]. Therefore, it is anticipated the trapped electrons would reach the deceleration phase of the wakefield. However, this is not the case as long as we consider the downward density transition in the parabolic density channel in which increased plasma wavelength can keep the trapped electrons effectively in the acceleration phase of the wakefield. While being accelerated, the trapped electrons have shown so-called “betatron” motion [16], in which their transverse amplitude is continuously varied from maximum to minimum in the wakefield. On the other hand, as the laser wakefield passes through the upward density transition of the parabolic density profile, quite different phenomena are anticipated since the plasma wavelength (λ_p) decreases, the very front portion of the accelerated electrons may be gradually laid in the deceleration phase of the wake field (i.e., slippage or detuning) [11]. It should be noted that, however, in our simulation except for the very few front part of the electron beam most of the electrons are still in the acceleration phase of the wakefield,

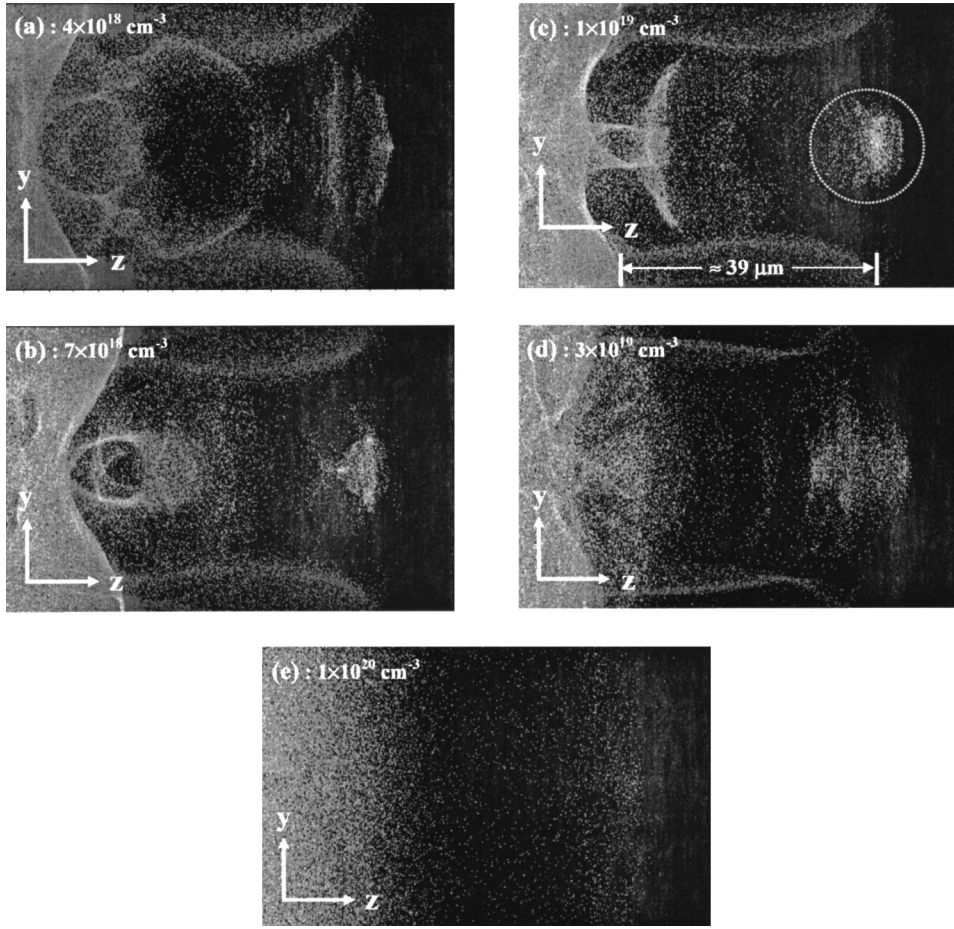


FIG. 3. Examples of typical shapes of the electron bunch emitted from the plasma channel [i.e., 4×10^{18} (a), 7×10^{18} (b), 1×10^{19} (c), 3×10^{19} (d), and $1 \times 10^{20} \text{ cm}^{-3}$ (e), respectively] when 20 TW laser pulse was used in these simulations.

gaining more energy from the field. These results can be explained by the “accordion effect” of Katsouleas *et al.* [17]; when a laser propagates in a tapered plasma channel the plasma density (n_e) increases, the plasma wavelength (λ_p) decreases, but the phase velocity of the wakefield increases [17]. Thus, a plasma density increase can increase the wake phase velocity and thereby avoid electron slippage but the dephasing length is anticipated to be larger in the tapered channel. This effect has been recently described by Sprangle *et al.* [18] for a laser propagating in a tapered plasma channel.

In order to observe the characteristics of the trapped electron bunches with respect to the laser power, five plasma densities (i.e., 4×10^{18} , 7×10^{18} , 1×10^{19} , 3×10^{19} , and $1 \times 10^{20} \text{ cm}^{-3}$) were used in the simulations with 10, 20, and 30 TW laser powers. Figure 3 shows examples of typical shapes of the electron bunch emitted from the plasma channel [i.e., 4×10^{18} (a), 7×10^{18} (b), 1×10^{19} (c), 3×10^{19} (d), and $1 \times 10^{20} \text{ cm}^{-3}$ (e), respectively] when 20 TW laser pulse was used in this simulations. The electron bunch is in vacuum now and the location of the electron bunch is approximately $\approx 39 \mu\text{m}$ away from the end of the plasma channel. These electron bunches can be picked out by using a magnetic field after it is emitted from the plasma. Unless otherwise stated the location of the electron bunch investigated in this simulation is approximately $\approx 39 \mu\text{m}$ away from the end of the plasma channel.

We now focus our attention on the electron bunches sur-

rounded by a dashed circle noted in Fig. 3(c). Physical quantities of the electron bunch including total charge (Q_b), average energy \bar{E} , r.m.s. (root-mean-square) energy spread, which is defined by $\Delta E_{\text{r.m.s.}}/\bar{E}$, r.m.s. bunch radius (r_b), r.m.s. bunch duration (τ_b), and normalized emittances (ϵ_n) were obtained from the simulation as functions of the plasma density and laser power. In order to get those physical quantities stated above, total numbers of the trapped electrons in the bunch should be calculated by using the following equation [19,20]:

$$N = (\bar{N}/N_0)n_e dx_1 dx_2 \Delta x_3 [c/w_p]^3.$$

Here, N is the total number of the trapped simulation particles, $N_0=4$ is the number of particles per cell used in the simulations, n_e is the average electron density in cm^{-3} , dx_1 and dx_2 are the cell sizes in the longitudinal and transverse directions, Δx_3 is the assumed extension in the third spatial dimension, and w_p is the plasma oscillation frequency. dx_1 and dx_2 , Δx_3 are in normalized units. We assume that Δx_3 is equal to Δx_2 , the width of accelerated beam in x_2 , which assumes cylindrical symmetry for the accelerated beam.

The characteristics of the electron bunch are investigated and the results are shown in Fig. 4 as functions of laser power and plasma density. Here, Figs. 4(a), 4(b), and 4(c) represent the results for 10, 20, and 30 TW laser power, respectively. Again, it includes average energy \bar{E} , total

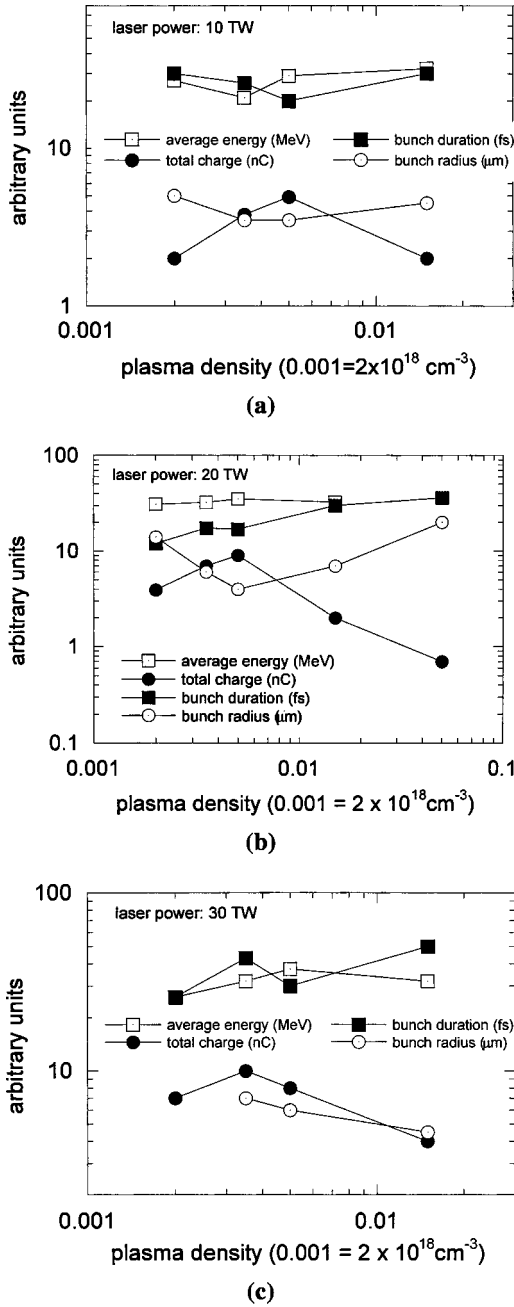


FIG. 4. Characteristics of the electron bunch investigated in this simulation as functions of laser power and plasma density. It includes average energy (MeV), total charge (nC), r.m.s. bunch duration (fs), and r.m.s. bunch radius (μm). Here, (a) is for 10 TW, (b) is for 20 TW, and (c) is for 30 TW, respectively.

charge (Q_b), r.m.s. bunch radius (r_b), and r.m.s. bunch duration (τ_b). Overall r.m.s. energy spread (i.e., $\Delta E_{\text{r.m.s.}}/\bar{E}$) of the electron bunches calculated in this simulation ranged from 18 to 31%. As shown in Figs. 4(a) and 4(b) the total charge of the electron bunch shows peak values of $Q_b \approx 4.9$ and 9 nC for 10 and 20 TW of laser power, respectively, and also shows relatively higher average energies of $\bar{E} \approx 28.8$ and 35 MeV at the plasma density of 0.005 (i.e., $1 \times 10^{19} \text{ cm}^{-3}$). Moreover, the r.m.s. bunch radius, which is

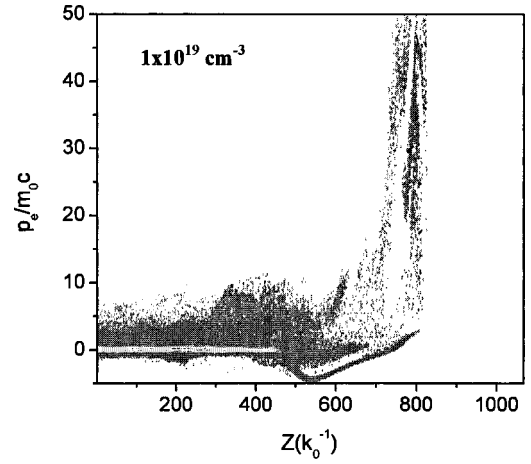


FIG. 5. An example of the simulation result of the momentum phase space (p_z, z), which corresponds directly to the $\times 2 \times 1$ phase space of Fig. 3(c).

closely related to the normalized emittance (ϵ_n), shows a minimum value of $r_b \approx 3.5$ and $4.0 \mu\text{m}$ for laser powers of 10 and 20 TW, respectively. This result is illustrated in Fig. 3(c) as the electron bunch in the simulations shows bright and smaller size compared to the others. It is interesting to note that the general trend of the r.m.s. bunch radius is much different from that of the total charge of the electron bunch for both the 10 and 20 TW laser power cases. However, for the 30 TW case, while the average energy shows a maximum of $\bar{E} \approx 37.5$ MeV at the plasma density of 0.005 (i.e., $1 \times 10^{19} \text{ cm}^{-3}$) the total charge of the electron bunch shows its maximum of $Q_b \approx 10$ nC at the plasma density of 0.0035 (i.e., $7 \times 10^{18} \text{ cm}^{-3}$). Also, the minimum r.m.s. bunch radius observed in the highest total charge for the 10 and 20 TW is not applicable in this case.

Figure 5 shows one example of the simulation result of the momentum phase space (p_z, z), which corresponds directly to the $\times 2 \times 1$ phase space of Fig. 3(c). Results show that the accelerated electron bunch [denoted as a dotted circle in Fig. 3(c)] has momenta in the ranges of 5 and 25 MeV/c and the r.m.s. bunch duration $\tau_b \approx 17$ fs, which corresponds to $\approx 5 \mu\text{m}$ in bunch length. However, it should be pointed out that the accelerated electron bunch shows large energy spread, which is due to the dephasing of the electron bunch to the laser wakefield [11], and it is commonly observed elsewhere [8].

The normalized emittance (ϵ_n) of the electron bunches are calculated from $\epsilon_n = \gamma_0 r_b \theta_b$, where γ_0 , r_b , and θ_b are the Lorentz factor of the average energy, r.m.s. bunch radius, and angular spread of the electron bunch, respectively, and the results are shown in Fig. 6. Again, it should be noted that the normalized emittance is calculated for the electron bunches, which are located in exactly the same distance indicated in Fig. 3(c) (i.e., $\approx 39 \mu\text{m}$ away from the plasma channel). As shown in Fig. 6, it is clear that at a specific laser power one can find a corresponding plasma density, which satisfies the normalized emittance growth to be minimum. For example, at laser powers of 10, 20, and 30 TW, the corresponding plasma densities that fulfill the normalized emittance growth to be minimum are 7×10^{18} , 1×10^{19} , and

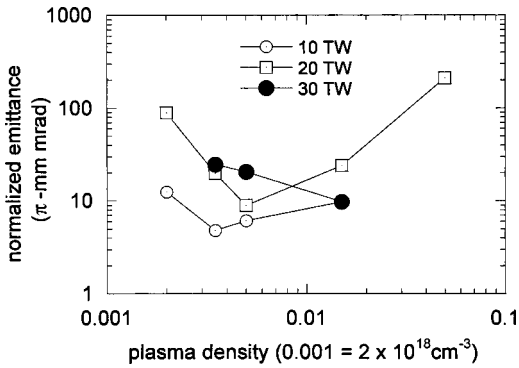


FIG. 6. The normalized emittance (ε_n) of the electron bunches calculated from $\varepsilon_n = \gamma_0 r_b \theta_b$, where γ_0 , r_b , and θ_b are the Lorentz factor of the average energy, r.m.s. bunch radius, and angular spread of the electron bunch, respectively.

$3 \times 10^{19} \text{ cm}^{-3}$, respectively, and they tend to increase with the laser power as shown in Fig. 7.

IV. CONCLUSIONS

In conclusion, a 2D PIC simulation study was performed to investigate the electron self-trapping and acceleration in a plasma by using a simple parabolic density model, in which the scale length of the plasma density transition is larger than Suk's scheme [8] but smaller than Bulanov's [10]. Physical quantities of the electron bunches emitted from the plasma were characterized as functions of plasma density and laser power. It includes average energy \bar{E} , total charges (Q_b) of the electron bunch, r.m.s. bunch radius (r_b), r.m.s. bunch

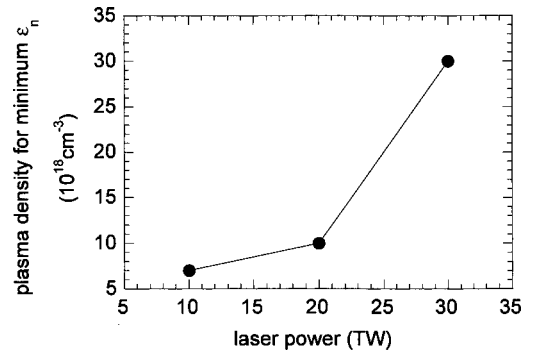


FIG. 7. Plasma densities that fulfill the normalized emittance growth to be minimum.

duration (τ_b), r.m.s. energy spread (i.e., $\Delta E_{\text{r.m.s.}}/\bar{E}$), and normalized emittance (ε_n) of the electron bunches.

Despite the large momentum spread, the trapped electrons can be effectively accelerated with momenta in the range of 5–20 MeV/c, which is similar to the previous results that used sharp downward density transition [8]. It is anticipated that the present work proposes an experimentally easier and more feasible method for the electron trapping and acceleration in a plasma.

ACKNOWLEDGMENTS

The authors would like to thank Professor W. Mori at UCLA for the OSIRIS code. This work was supported by the Korean Ministry of Science and Technologies through the Creative Research Initiative Program.

-
- [1] T. Tajima and J. M. Dawson, Phys. Rev. Lett. **43**, 267 (1979).
 [2] S. V. Bulanov, V. I. Kirsanov, and A. S. Sakharov, JETP Lett. **50**, 198 (1989).
 [3] P. Sprangle, E. Esarey, and A. Ting, Phys. Rev. Lett. **64**, 2011 (1990).
 [4] H. Hamster, A. Sullivan, S. Gordon, W. White, and R. W. Falcone, Phys. Rev. Lett. **71**, 2725 (1993).
 [5] J. R. Marques, J. P. Geindre, F. Amiranoff, P. Audebert, J. C. Gauthier, A. Antonetti, and G. Grillon, Phys. Rev. Lett. **76**, 3566 (1996).
 [6] D. Umstadter, J. K. Kim, and E. Dodd, Phys. Rev. Lett. **76**, 2073 (1996).
 [7] E. Esarey, R. F. Hubbard, W. P. Leemans, A. Ting, and P. Sprangle, Phys. Rev. Lett. **79**, 2682 (1997).
 [8] H. Suk, N. Barov, J. B. Rosenzweig, and E. Esarey, Phys. Rev. Lett. **86**, 1011 (2001).
 [9] K. Nakajima *et al.*, Phys. Rev. Lett. **74**, 4428 (1995).
 [10] S. V. Bulanov, N. Naumova, F. Pegoraro, and J. Sakai, Phys. Rev. E **58**, R5257 (1998).
 [11] E. Esarey, P. Sprangle, J. Krall, and A. Ting, IEEE Trans. Plasma Sci. **24**, 252 (1996).
 [12] H. Suk, G. H. Kim, J. U. Kim, C. Kim, J. Kim, and H. J. Lee (unpublished).
 [13] R. N. Agarwal, V. K. Tripathi, and P. C. Agarwal, IEEE Trans. Plasma Sci. **24**, 143 (1996).
 [14] R. G. Hemker, Ph.D. thesis, UCLA, Los Angeles, 2000.
 [15] J. U. Kim, H. J. Lee, C. Kim, G. H. Kim, and H. Suk, J. Appl. Phys. **94**, 5497 (2003).
 [16] E. Esarey, B. A. Shadwick, P. Catravas, and W. P. Leemans, Phys. Rev. E **65**, 056505 (2002).
 [17] T. Katsouleas, Phys. Rev. A **33**, 2056 (1986).
 [18] P. Sprangle *et al.*, Phys. Rev. E **63**, 056405 (2001).
 [19] R. Hemker *et al.*, Phys. Rev. E **57**, 5920 (1998).
 [20] N. Hafz, H. J. Lee, J. U. Kim, G. H. Kim, and H. Suk (unpublished).